Int. J. Electrochem. Sci., 15 **(2020)** 11479 – 11492, doi: 10.20964/2020.11.31

International Journal of
ELECTROCHEMICAL
SCIENCE
www.electrochemsci.org

Amino Acid-Functionalized Electrochemically Reduced Graphene Oxide-Modified Glassy Carbon Electrodes for the Efficient Sensing of Nitrite

Peilong Wang[1,2], *Xiao Liu*[1], *Wei Ma*[1], *Gen Liu*[1,*] *and Hui Gao*[1,*]

[1] School of Chemistry and Materials Science, Huaibei Normal University, Huaibei, Anhui 235000, China
[2] Information School, Huaibei Normal University, Huaibei, Anhui 235000, China
[*]E-mail: liugen7084@126.com; gaohuichem@chnu.edu.cn

Received: 30 July 2020 / *Accepted:* 1 September 2020 / *Published:* 30 September 2020

In this work, different structures of amino acid-functionalized electrochemically reduced graphene oxide-modified glassy carbon electrodes (ERGO/GCEs) were developed and applied for the determination of nitrite. L-arginine (L-Arg), L-tyrosine (L-Tyr) and L-histidine (L-His), which are aliphatic, aromatic, and heterocyclic amino acids, respectively, were selected for this work, and the corresponding electrodes were L-Arg-ERGO/GCE, L-Tyr-ERGO/GCE, and L-His-ERGO/GCE**.** The sensing capabilities of the modified electrodes were characterized by electrochemical impedance spectroscopy (EIS), cyclic voltammetry (CV), and differential pulse voltammetry (DPV). The comparative results indicated the outstanding performance of L-histidine with an enhanced electrochemical signal for nitrite due to its powerful imidazole groups, π-π interactions and lone pair-π interactions.

Keywords: L-arginine, L-tyrosine, L-histidine; graphene, modified electrode, nitrite

1. INTRODUCTION

Research on chemically modified electrodes is currently one of the most active trends in electrochemistry. Numerous modified electrode materials have been developed to improve electrochemical detection performance [1]. Amino acids, a group of organic molecules that consist of a basic amino group (—NH_2), an acidic carboxyl group (—COOH), and an organic R group (or side chain), have many unique properties; thus, amino acids have attracted the attention of researchers. When utilized as electrode modifiers, amino acids have many inherent advantages, such as their low price, easy access, good reproducibility, high stability, large active sites, uniform deposition and easy adhesion to the electrode surface [2]. When amino acids are modified to the electrode surface by chemical methods or electrochemical methods, they show unique superiority in the determination of metal ions,

biomolecules, organic pollutants and so on. To date, a variety of amino acids such as L-cysteine [3-7], L-lysine [8-12], L-methionine [13-15], L-arginine [16-19], glutamic acid [20-23], L-tryptophan [24], alanine [25], threonine [26], L-valine [27], L-tyrosine [28-30], and L-histidine [31-34] have mostly been utilized as electrode modifiers. Moreover, graphene is a new type of two-dimensional carbon nanomaterial that has the advantages of a large specific surface area, high electrical conductivity, and good catalytic activity [35]. It can be used as a base material for supporting metal particles with electrocatalytic activity, conductive polymer materials, etc. to further synergistically increase catalytic performance. At present, the composite modified electrode of amino acids and graphene has also become a good electrochemical sensor [36-39].

Nitrite is ubiquitous in food, drinking water and the environment and can interact with proteins to produce highly carcinogenic nitrosamines [40]. An excessive intake of nitrite can cause many health problems, such as gastric and esophageal cancer [41], infant methemoglobinemia (blue baby syndrome) [42], and spontaneous abortion [43]. Nitrite is an electrically active substance, and electrochemical detection methods [44] have the advantages of being simple, fast, sensitive, and economical. Nitrite demonstrates electrical activity on the surface of platinum, gold, copper, glassy carbon, and transition metal oxide electrodes, but because an electrode surface can be easily contaminated, the detection sensitivity and accuracy decrease, which limits the detection of nitrite in practical applications [45]. The necessary modification of the electrode surface can not only increase the response signal of the nitrite oxidation reaction but also broaden the dynamic range of detection. The electrode modification materials that have been reported include graphene [46], carbon nanotubes [47], carbon nanoparticles [48], porous carbon [49] and other carbon materials; metals [50], metal oxides [51], metal sulfide [52], metal nitride nanoparticles [53] and other metal materials; metal organic frameworks (MOFs) [54]; and conductive polymers [55], enzymes [53], as well as other various composite materials [56]. Among them, nitrogen-doped graphene [57], metals [56], metal oxides [58], polymers [59], MOFs [54], enzymes [60] and other graphene nanocomposites have been reported for the construction of nitrite electrochemical sensors. However, nanocomposites of amino acids and graphene have not been reported for the construction of nitrite electrochemical sensors.

In the current work, three amino acid- functionalized electrochemically reduced graphene oxide-modified electrodes were developed as nitrite sensors. L-arginine, L-tyrosine and L-histidine were selected as representatives of the aliphatic, heterocyclic and aromatic groups, and their corresponding structures are shown in Figure 1.

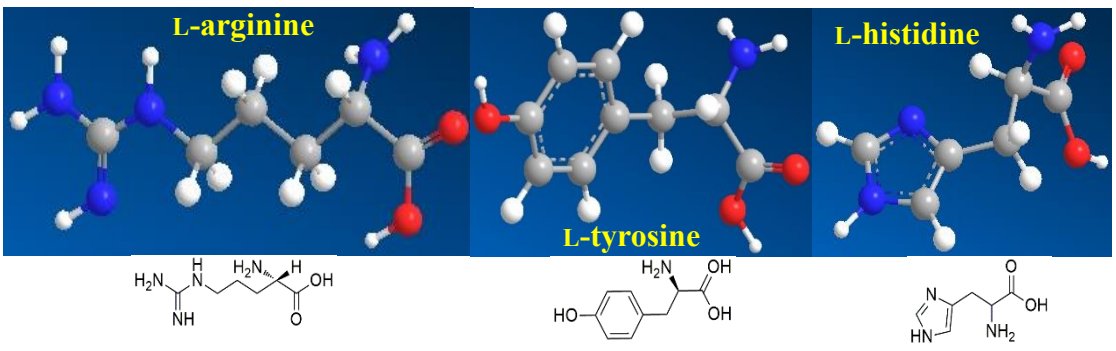

Figure 1. Chemical structures of L-arginine, L-tyrosine and L-histidine.

2. EXPERIMENTAL

2.1 Apparatus

The electrochemical impedance spectra (EIS) were detected on a CHI760E (Chen-hua, Shanghai, China) electrochemical workstation. Cyclic voltammograms (CV) and differential pulse voltammograms (DPV) were performed on an LK2006A electrochemical workstation (Tianjin Lanlike Chemical Electronics High Technology Co., Ltd.). These two electrochemical workstations consist of a glassy carbon electrode working electrode, a platinum counter electrode, and a KCl-saturated Ag/AgCl reference electrode. A Quanta 450 microscope (JSM-6610LV, JEOL, Japan) was used for conducting scanning electron microscopy (SEM). Acidity measurements were carried out using a digital pH/mV meter (PHS-3C, Shanghai Leici Device Works, China). All experiments in this work were performed at room temperature.

2.2 Reagents

A graphene oxide dispersion (2 mg/mL) was obtained from XFNANO Materials Technology Co. (Nanjing, China). L-arginine, L-tyrosine, L-histidine and nitrite were purchased from Bio Life Science & Technology Co. (Shanghai, China). Amino acid and nitrite stock solutions with concentrations of 2.5 × 10^{-3} mol L^{-1} and 1.0 × 10^{-3} mol L^{-1}, repectively were prepared. Phosphate-buffered saline (PBS) solutions were prepared with 0.1 mol L^{-1} H_3PO_4, NaOH, and Na_2HPO_4-NaH_2PO_4. All solutions were prepared by double-distilled water. All chemicals are analytical grade.

2.3 Preparation of modified electrode

A bare GCE was polished with 0.05 μm alumina powder and rinsed in double-distilled water. Then, the polished electrode was sequentially sonicated in absolute ethanol and double-distilled water. The cleaned GCE was dried in air. CV was used to prepare the modified electrode. A polymerization solution was prepared by mixing the graphene dispersion, 2.5 × 10^{-3} mol L^{-1} of a corresponding amino acid solution, and a phosphate-buffered saline solution (L-arginine at pH 5.5, L-tyrosine at pH 8.5, and L-histidine at pH 8.0) at a ratio of 2:1:1. The L-Arg-ERGO/GCE was electropolymerized by potential cycling from -0.8 to 2.4 V at 100 mV s^{-1} for 9 cycles. The L-tyrosine was electropolymerized by potential cycling from -0.8 to 2.2 V at 80 mV s^{-1} for 10 cycles. Finally, the L-histidine was electropolymerized by repetitive potential cycling from -1.6 to 1.8 V at 80 mV s^{-1} for 8 cycles. After polymerization, the three modified electrodes were rinsed with double-distilled water and then air dried.

2.4 Sample preparation

A 10 g sample, weighed by an electronic balance, was pulverized and added 70 mL double-distilled water and 12 mL of NaOH in order, before being diluted to 250 mL. Next, 10 mL of the $ZnSO_4$ solution was added to the above solution, shaken well, adjusted to be weakly alkaline, and heat treated

in a 60 ^{0}C water bath for 10 min. After cooling to room temperature, the above solution was diluted and filtered, and then the filtrate was collected after discarding 20 mL of the initial filtrate.

2.5 Analytical method

To obtain a stable voltammogram, the modified electrodes were activated by CV in 10 mL of blank solution (5 mL of pH 7.0 PBS and 5 mL of double-distilled water) before every electrolysis test. The optimized CV parameters for L-Arg-ERGO/GCE were a 0.3-1.2 V potential range, 120 mV s^{-1} scan rate, and 5 s wait time. The optimized CV parameters for L-Tyr-ERGO/GCE were a 0.2-1.4 V potential range, 180 mV s^{-1} scan rate, and 5 s wait time. Finally, the optimized CV parameters for L-His-ERGO/GCE were a 0.2-1.3 V potential range, 180 mV s^{-1} scan rate, and 5 s wait time. The optimized DPV parameters for L-Arg-ERGO/GCE were a 0.3-1.3 V potential range, 7 mV potential increase, 90 mV pulse amplitude, 60 ms pulse width, 100 ms pulse interval, and 30 s wait time. The optimized DPV parameters for L-Tyr-ERGO/GCE were a 0.2-1.3 V potential range, 3 mV potential increase, 90 mV pulse amplitude, 70 ms pulse width, 300 ms pulse interval, and 10 s wait time. Finally, the optimized DPV parameters for L-His-ERGO/GCE were a 0.4-1.2 V potential range, 6 mV potential increase, 90 mV pulse amplitude, 50 ms pulse width, 300 ms pulse interval, and 5 s wait time.

3. RESULTS AND DISCUSSION

3.1 Identification of L-Arg-ERGO/GCE, L-Tyr-ERGO/GCE, and L-His-ERGO/GCE

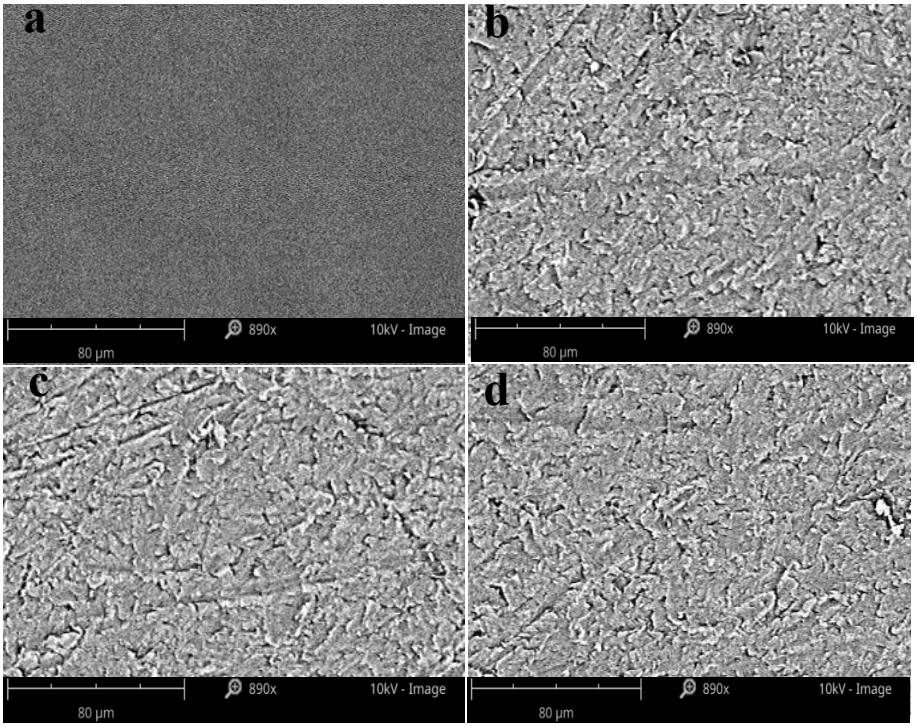

Figure 2. SEM images of the bare GCE (a), L-Arg-ERGO/GCE (b), L-Tyr-ERGO/GCE (c), and L-His-ERGO/GCE (d).

The morphologies of the bare GCE and the modified electrodes were characterized by SEM. Compared with the bare GCE (Figure 2a), L-Arg-ERGO/GCE (Figure 2b), L-Tyr-ERGO/GCE (Figure 2c), and L-His-ERGO/GCE (Figure 2d) showed thin and crumpled surface sheets with nanometer-scale bulges. These results support the existence of amino acids and reduced graphene on the surface of the GCE, which is consistent with what has been reported in the literature [61]. This characteristic indicates that the modifiers completely adhered to the electrode surfaces, which is helpful in maintaining an effective surface area on the electrode and accelerating the electron transfer rate.

3.2. Electrochemical characterization of L-Arg-ERGO/GCE, L-Tyr-ERGO/GCE, and L-His-ERGO/GCE

EIS is a powerful method to study diffusion effects at the modified electrodes [62], and was selected to evaluate the electron transfer abilities of the three modified electrodes. Figure 3 depicts the electrochemical impedance spectra of the bare GCE (a), L-Arg-ERGO/GCE (b), L-Tyr-ERGO/GCE (c), and L-His-ERGO/GCE (d) in a 0.1 mol L^{-1} KCl solution containing 5.0×10^{-3} mol L^{-1} $Fe(CN)_6^{3-/4-}$. The semicircle diameter in the EIS spectrum represents the electron transfer resistance (Rct) [63]. High semicircle portions correspond to an electron transfer-limited process and a low frequency corresponds to a controlled diffusion process [64]. The smaller resistances of the three modified electrodes compared with the bare GCE demonstrates that the combination of ERGO and amino acids can provide more electroactive sites. Moreover, the electron-transfer rate of L-His-ERGO/GCE is found to be relatively larger than that of L-Arg-ERGO/GCE and L-Tyr-ERGO/GCE. Therefore, L-histidine can be strongly attached to the surface of the GCE by lipophilic π-π conjugated interactions of the side imidazole groups.

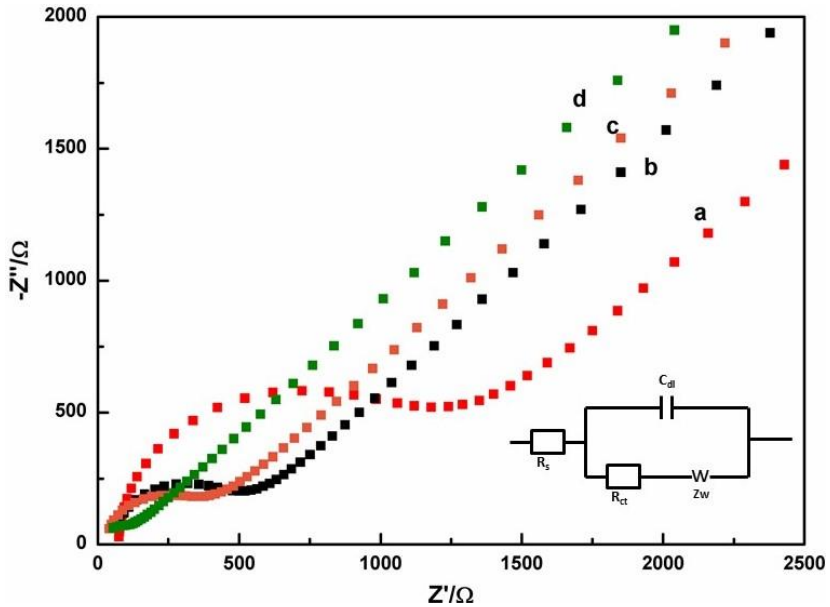

Figure 3. Electrochemical impedance spectra of the bare GCE (a), L-Arg-ERGO/GCE (b), L-Tyr-ERGO/GCE (c), and L-His-ERGO/GCE (d) in a 0.1 mol L^{-1} KCl solution containing 5.0×10^{-3} mol L^{-1} $Fe(CN)_6^{3-/4-}$. The illustration shows the Randle equivalent circuit.

Both π-π and lone pair-π interactions play a pivotal role in the electron transfer process [65, 66], and L-histidine combined with ERGO can dramatically improve the electron transfer efficiency. Although tyrosine also contains π-π and pair-π bonds, it is a seven-center, eight-electron system. Thus, the electron cloud density of tyrosine is lower than that of histidine, which has five centers and six electrons. Therefore, the electron transfer effect of tyrosine is inferior to that of histidine. Although arginine has a more flexible structure and is easy to attach to the electrode surface, its electron transfer ability is still unsatisfactory because it does not contain π-π and pair-π interactions. These observations indicate that L-His-ERGO/GCE has superior conductivity and is more suitable as an electrochemical sensor.

3.3 Electrochemical response of L-Arg-ERGO/GCE, L-Tyr-ERGO/GCE, and L-His-ERGO/GCE to nitrite

3.3.1. Voltammetric behaviors of the three differently modified electrodes to nitrite

The electrochemical behavior of 5.00×10^{-4} mol L^{-1} nitrite at the different electrodes was investigated, as shown in Figure 4. Figure 4 depicts the cyclic voltammograms of the bare GCE (a), L-Arg-ERGO/GCE (b), L-Tyr-ERGO/GCE (c), and L-His-ERGO/GCE (d), and the oxidation peaks appear at 1.018, 0.906, 0.918 and 0.921 V, respectively. The three modified electrodes show an enhanced oxidation peak compared to that of the bare GCE. This result can be explained by the fact that the employed amino acid and ERGO composite modifiers can catalyze the oxidation of nitrite. Furthermore, the oxidation peak of nitrite at the L-His-ERGO/GCE is found to be higher than that of L-Arg-ERGO/GCE and L-Tyr-ERGO/GCE, which indicates that L-His-ERGO/GCE can supply a necessary pathway for electron transfer from nitrite to the electrode. This result shows that L-His-ERGO/GCE has better selectivity in the determination of nitrite ions.

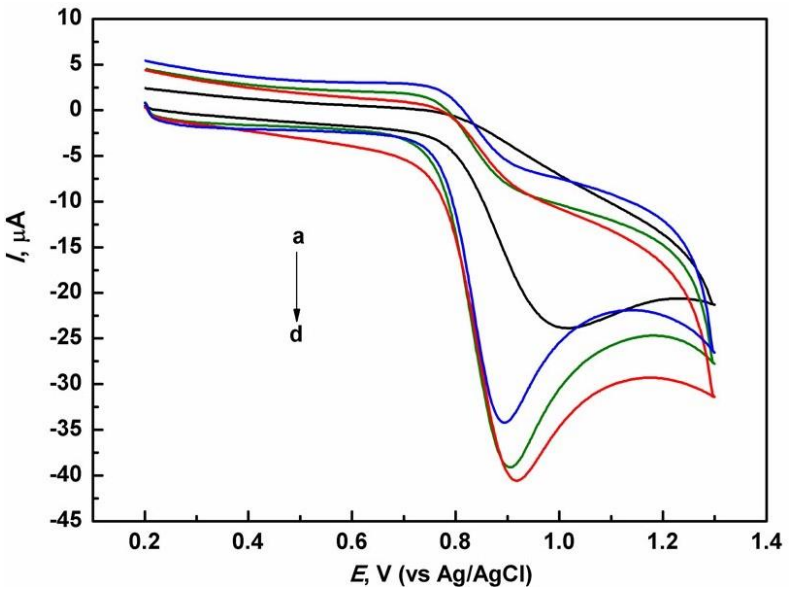

Figure 4. Cyclic voltammograms of 5.00×10^{-4} mol L^{-1} nitrite at the bare GCE (a), L-Arg-ERGO/GCE (b), L-Tyr-ERGO/GCE (c), and L-His-ERGO/GCE (d).

3.3.2. Influence of scan rate

The influence of scan rate on the electrochemical oxidation of 5.00×10^{-4} mol L^{-1} nitrite at L-Arg-ERGO/GCE, L-Tyr-ERGO/GCE, and L-His-ERGO/GCE was analysed by CV with scan rates from 0.02 to 0.4 V/s (Figure 5). The linear regression equations between the scan rates, peak currents, and peak potentials are listed in Table 1. The slopes of the log*I*–log*v* equations are all approximately 0.5, demonstrating that the oxidation of nitrite at the three modified electrodes is a diffusion-controlled process, as observed by other authors [50]. The slope of *E*p–ln*v* equation is usually used to estimate the number of reaction electrons. According to Laviron's theory [67], two reaction electrons are calculated in the oxidation of nitrite at L-Arg-ERGO/GCE, L-Tyr-ERGO/GCE, and L-His-ERGO/GCE.

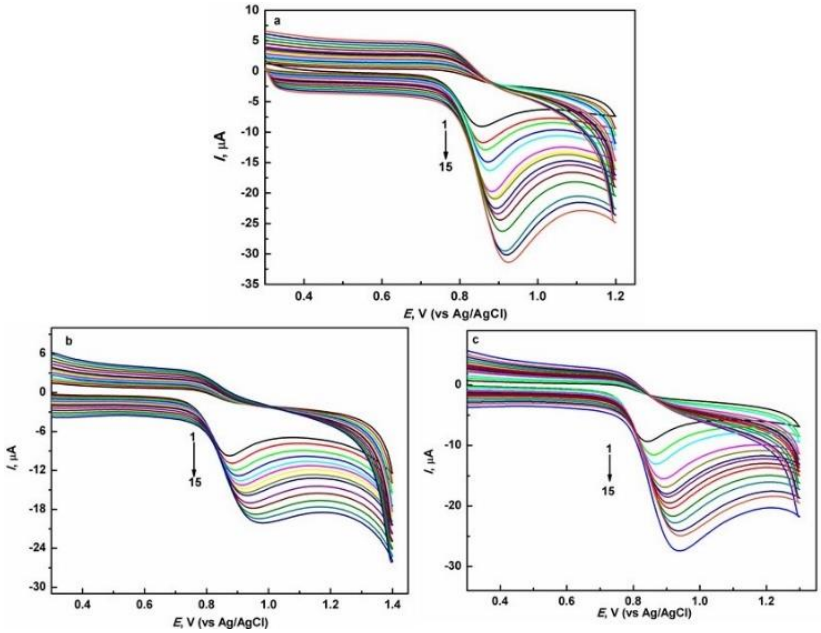

Figure 5. CVs of 5.00×10^{-4} mol L^{-1} nitrite at L-Arg-ERGO/GCE (a), L-Tyr-ERGO/GCE (b), and L-His-ERGO/GCE (c) at different scan rates (1-15): 20, 40, 60, 80, 100, 120, 140, 160, 180, 200, 240, 280, 320, 360, and 400 mV s^{-1}.

Table 1. Relationship between the scan rate and peak current and the scan rate and peak potential

Peak current			Peak potential		
Electrodes	Linear regression equation, *I*, μA; *v*, V/s	Correlation coefficient	Electrodes	Linear regression equation, *E*, V; *v*, V/s	Correlation coefficient
L-Arg-ERGO/GCE	$\lg I_{Pa} = 1.3353 + 0.4965 \lg v$	0.9962	L-Arg-ERGO/GCE	Epa =0.9032+ 0.03238ln$v$	0.9910
L-Tyr-ERGO/GCE	$\lg I_{Pa} = 1.4922 + 0.5053 \lg v$	0.9933	L-Tyr-ERGO/GCE	Epa =0.9256 + 0.03086ln$v$	0.9920
L-His-ERGO/GCE	$\lg I_{Pa} = 1.6052+ 0.5024 \lg v$	0.9983	L-His-ERGO/GCE	Epa = 0.8928 + 0.03195ln$v$	0.9935

3.3.3 Diffusion coefficient of the three different modified electrodes to nitrite

Chronoamperometry was applied to investigate the diffusion capacity of nitrite on the different electrodes. The corresponding diffusion coefficients were calculated using the Cottrell equation, and the results are shown in Table 2. For the bare GCE, L-Arg-ERGO/GCE, L-Tyr-ERGO/GCE, and L-His-ERGO/GCE, the diffusion coefficients increase sequentially. The largest diffusion coefficient is on the surface of L-His-ERGO/GCE and indicates the best electrochemical response.

Table 2. Diffusion coefficient of nitrite at the different electrodes

Electrodes	Bare GCE	L-Arg-ERGO/GCE	L-Tyr-ERGO/GCE	L-His-ERGO/GCE
D (cm^2/s)	2.44×10^{-6}	5.05×10^{-6}	6.12×10^{-6}	7.07×10^{-6}

3.3.4 Influence of solution pH

The pH value of the supporting electrolyte has a significant influence in electrochemical studies by varying both the peak potential and peak current [36]. The influence of solution pH on the nitrite electrochemical response at the three modified electrodes was investigated by CV in a pH ranges of 2.0-7.0. AT the L-Arg-ERGO/GCE, L-Tyr-ERGO/GCE, and L-His-ERGO/GCE, the highest peak currents of nitrite appeared at pH 3.5. The peak potentials negatively shift with an increase in pH, indicating that protons participate in the nitrite oxidation process, as suggested in the earlier studies [68]. The *E*–pH relationship of nitrite at L-Arg-ERGO/GCE, L-Tyr-ERGO/GCE, and L-His-ERGO/GCE can be expressed with the following equations: *E*pa (V) = 1.0078 – 0.0568pH (r = 0.9952), *E*pa (V) =1.0005 – 0.0585 pH (r = 0.9934); *E*pa (V) =1.0315 – 0.0578 pH (r = 0.9972). Based on the slope values (all values are close to 0.059), two protons are involved in the oxidation process according to the two theoretically computed electron numbers. Considering the good peak current and peak shape, a pH of 3.5 is chosen as the optimum determination condition.

3.4 Application

3.4.1 Calibration curve

The relationship between the electrochemical response and nitrite concentration was determined by CV and DPV techniques with the three modified electrodes. Figure 6 shows the CV and DPV responses at the three modified electrodes while varying the nitrite concentration. The corresponding linear ranges, linear regression equations, and detection limits are presented in Table 3. It can be clearly seen that the linear range and detection limit obtained by DPV at L-His-ERGO/GCE were even better than those detected at L-Arg-ERGO/GCE and L-Tyr-ERGO/GCE. The performance of the L-His-

ERGO/GCE is compared with that of other sensors for nitrite detection, and the results are shown in Table 4. It can be seen from the table that this work has obvious advantages in the detection limit. Compared with those of CS/MWCNTs/CNs/GC [48] and HPG/GCE [49], the improved results of L-His-ERGO/GCE are more clear.

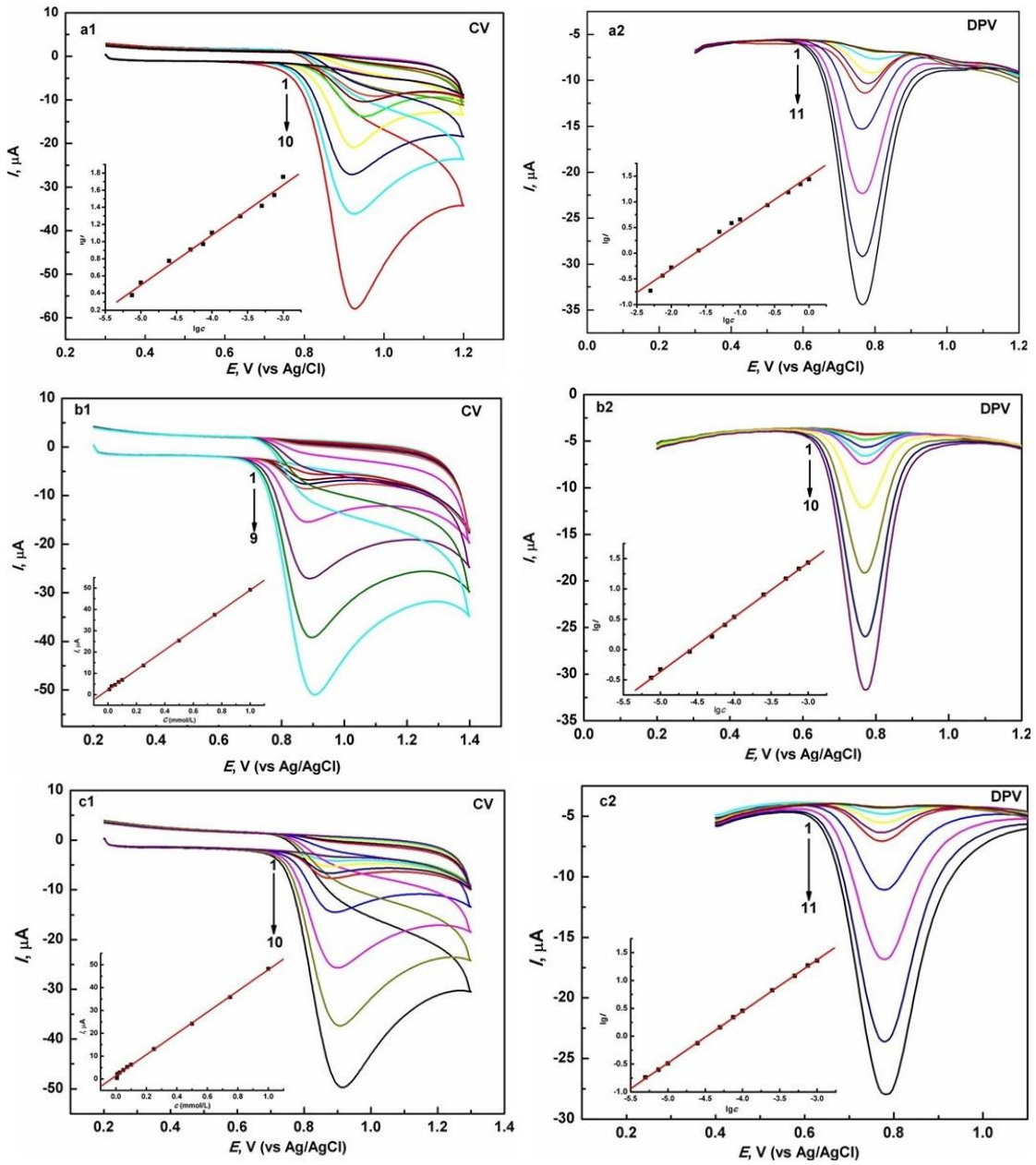

Figure 6. CVs (a1) and DPVs (a2) of nitrite at various concentrations at L-Arg-ERGO/GCE (inset is the plot of the oxidation peak current of nitrite versus its concentration). The numbers in (a1) from 1 to 10 corresponds to concentrations of 8.00×10^{-6}, 1.20×10^{-5}, 4.80×10^{-5}, 7.20×10^{-5}, 9.60×10^{-5}, 1.20×10^{-4}, 2.40×10^{-4}, 4.60×10^{-4}, 6.60×10^{-4}, and 8.60×10^{-4}mol L^{-1}, respectively. The numbers in (a2) from 1 to 11 corresponds to concentrations of 8.00×10^{-6}, 1.20×10^{-5}, 4.80×10^{-5}, 7.20×10^{-5}, 9.60×10^{-5}, 1.20×10^{-4}, 2.40×10^{-4}, 4.60×10^{-4}, 6.60×10^{-4}, and 8.60×10^{-4} mol L^{-1}, respectively. CVs (b1) and DPVs (b2) of nitrite at various concentrations at the L-Tyr-ERGO/GCE (inset is the plot of the oxidation peak current of nitrite versus its concentration). The numbers in (b1) from 1 to 9 corresponds to concentrations of 8.00×10^{-6}, 1.20×10^{-5}, 4.80×10^{-5}, 7.20×10^{-5}, 9.60×10^{-5},

1.20×10^{-4}, 2.40×10^{-4}, 4.60×10^{-4}, 6.60×10^{-4}, and 8.60×10^{-4} mol L^{-1}, respectively. The numbers in (b2) from 1 to 10 corresponds to concentrations of 8.00×10^{-6}, 1.20×10^{-5}, 4.80×10^{-5}, 7.20×10^{-5}, 9.60×10^{-5}, 1.20×10^{-4}, 2.40×10^{-4}, 4.60×10^{-4}, 6.60×10^{-4}, and 8.60×10^{-4} mol L^{-1}, respectively. CVs (c1) and DPVs (c2) of nitrite at various concentrations at the L-His-ERGO/GCE (inset is the plot of the oxidation peak current of nitrite versus its concentration). The numbers in (c1) from 1 to 10 corresponds to concentrations of 8.00×10^{-6}, 1.20×10^{-5}, 4.80×10^{-5}, 7.20×10^{-5}, 9.60×10^{-5}, 1.20×10^{-4}, 2.40×10^{-4}, 4.60×10^{-4}, 6.60×10^{-4}, and 8.60×10^{-4} mol L^{-1}, respectively. The numbers in (c2) from 1 to 11 corresponds to concentrations of 8.00×10^{-6}, 1.20×10^{-5}, 4.80×10^{-5}, 7.20×10^{-5}, 9.60×10^{-5}, 1.20×10^{-4}, 2.40×10^{-4}, 4.60×10^{-4}, 6.60×10^{-4}, and 8.60×10^{-4} mol L^{-1}, respectively.

Table 3. Linear ranges, regression equation, correlation coefficient and detection limit for determination of nitrite on L-Arg-ERGO/GCE, L-Tyr-ERGO/GCE, and L-His-ERGO/GCE

Electrode	Method	Linear range (mol/L)	Linear regression equation, I (μA); c(mol/L)	Correlation coefficient	Detection limit (mol/L)
L-Arg-ERGO/GCE	CV	7.50×10^{-6}-1.00×10^{-3}	lg$I$=3.41047+0.58327lg$c$	0.99350	2.50×10^{-6}
	DPV	5.00×10^{-6}-1.00×10^{-3}	lg$I$=1.49522+0.90311lg$c$	0.99501	1.00×10^{-6}
L-Tyr-ERGO/GCE	CV	1.00×10^{-5}-1.00×10^{-3}	I=2.2593+4.68246c	0.99988	1.00×10^{-6}
	DPV	7.50×10^{-6}-1.00×10^{-3}	lg$I$=4.1315+0.89958lg$c$	0.99941	8.20×10^{-7}
L-His-ERGO/GCE	CV	7.50×10^{-6}-1.00×10^{-3}	I=1.33133+4.65112c	0.99948	9.00×10^{-7}
	DPV	5.00×10^{-6}-1.00×10^{-3}	lg$I$=4.1446+0.92471lg$c$	0.99987	1.00×10^{-7}

Table 4. Comparison of analytical performance of present sensor with other sensors reported in the literature

Modified electrode	Linear range (μM)	Detection limit (μM)	Technique used	Reference
[a] CS/MWCNTs/CNs/GC	5-1000	0.89	CV	[48]
[b] HPG/GCE	200-800 2000-10000	8.1	CV	[49]
[c] AgNS/GCE	0.1-8	0.031	Chronoampero	[50]

			metric	
[d] α-Fe_2O_3 NAs/CF/GCE	0.5-1000	0.12	Chronoampero metric	[51]
[e] Ni_7S_6/MWCNTs /GCE	1.0-4200	0.3	Chronoampero metric	[52]
L-His-ERGO/GCE	5-1000	0.1	DPV	This work

[a] Chitosan/Multi-walled carbon nanotubes/Carbon nanoparticles modified glassy carbon electrode
[b] hierarchically porous graphite modified glassy carbon electrode
[c] Silver nanospheres modified glassy carbon electrode
[d] α-Fe_2O_3 nanorod arrays (NAs)/carbon foam composite film coated glassy carbon electrode
[e] Ni_7S_6/Multi-walled carbon nanotubes film coated glassy carbon electrode

3.4.2 Reproducibility and stability

Two important parameters, namely, reproducibility and stability, are necessary to investigate for analytical determination [69]. To investigate the repeatability of the three differently modified electrodes, the corresponding DPVs with the 5.00×10^{-3} mol L^{-1} nitrite solution was repeatedly determined 15 times. The relative standard deviations (RSD) of the response currents from L-Arg-ERGO/GCE, L-Tyr-ERGO/GCE, and L-His-ERGO/GCE are 4.2, 3.5 and 3.2%, respectively. When the three modified electrodes are stored for 7 days at room temperature, the peak potentials and peak currents do not exhibit considerable changes, suggesting the remarkable reproducibility and long-term stability of the three modified electrodes. Compared to the other two modified electrodes, L-His-ERGO/GCE shows an advantage in repeatability experiments.

3.4.3 Interference studies

To evaluate the anti-interference ability of the three modified electrodes, possible interferents (all of them were 1 mg) were tested by analyzing 5.00×10^{-3} mol L^{-1} nitrite, and the relative errors were less than 5%. The experimental results showed that Ni^{2+}, Cu^{2+}, CO_3^{2-}, Zn^{2+}, Cl^-, EDTA, NO^{3-}, threonine, and ascorbic acid exhibit no interference with L-Arg-ERGO/GCE; Mn^{2+}, NO^{3-}, F^-, CH_3COO^-, Al^{3+}, Ni^{2+}, Cu^{2+}, CO_3^{2-}, Fe^{3+}, arginine, threonine, ascorbic acid, and sodium citrate exhibit no interference with L-Tyr-ERGO/GCE ; and SO_4^{2-}, CO_3^{2-}, Fe^{3+}, NO^{3-}, F^-, Cd^{2+}, Zn^{2+}, Cl^-, EDTA, sodium citrate, ascorbic acid and threonine exhibit no interference with L-His-ERGO/GCE. Therefore, a satisfactory anti-interference ability of the three modified electrodes is evident.

3.4.4 Determination of nitrite in natural samples

Nitrite in natural samples of ham, instant noodles, and sauerkraut were also detected by the three modified electrodes. The samples preparation is described in the Experimental section. For each sample, the original detected value, RSD, and recovery (calculated by the standard addition method) are listed in Table 5, and these results confirm that the three modified electrodes are suitable for practical applications. Moreover, L-His-ERGO/GCE has a better RSD and recovery than the other two modified electrodes, which indicates that it has better practical detection capabilities.

Table 5. Analysis results of nitrite in samples (*n*=5)

Electrodes	Sample	Original detected value (10^{-5} mol L^{-1})	Standard addition (10^{-5} mol L^{-1})	Detected total value after addition (10^{-5} mol L^{-1})	RSD (%)	Recovery (%)
L-Arg-ERGO/GCE	Ham	2.15	2.50	4.58	3.7	96.7
	Instant noodles	3.66	4.00	7.75	5.2	102.5
	Sauerkraut	4.22	4.00	8.11	4.3	97.3
L-Tyr-ERGO/GCE	Ham	1.00	1.00	2.03	4.5	103
	Instant noodles	4.25	5.00	9.35	2.7	102.4
	Sauerkraut	4.56	5.00	9.48	3.6	98.2
L-His-ERGO/GCE	Ham	1.86	2.50	4.41	4.2	102.7
	Instant noodles	4.07	5.00	8.98	2.6	97.8
	Sauerkraut	4.78	5.00	9.84	3.4	101.2

4. CONCLUSIONS

L-Arg-ERGO/GCE, L-Tyr-ERGO/GCE, and L-His-ERGO/GCE were proposed for the detection of nitrite. The prepared L-His-ERGO/GCE exhibited imidazole groups, π-π interactions and lone pair-π interactions, and this electrode showed excellent electrocatalytic activity and sensitivity towards nitrite. Moreover, he linear concentration range and the detection limit values obtained by L-His-ERGO/GCE were better than those obtained by L-Tyr-ERGO/GCE and L-Arg-ERGO/GCE. Additionally, the designed L-His-ERGO/GCE showed better analytical performance in real samples than the L-Arg-ERGO/GCE and L-Arg-ERGO/GCE, hence promoting its use as a promising electrochemical sensor.

ACKNOWLEDGEMENTS
This work was supported by the Key Project of Provincial Natural Science Research Foundation of Anhui Universities, China (No. KJ2018A0389 and KJ2018A0675); the Anhui Provincial Natural Science Foundation (No. 1808085QB29 and 2008085QB68); Foundation of State Key Laboratory of Analytical Chemistry for Life Science (Grants No. SKLACLS2003); Foundation of Henan Key Laboratory of Biomolecular Recognition and Sensing (Grants No. HKLBRSK1905).

References

1. L. Qiu, P. Lv, C. Zhao, X. Feng, G. Fang, J. Liu, and S. Wang, *Sens. Actuators, B*, 286 (2019) 386.
2. J. G. Manjunatha, *Heliyon,* 4 (2018) e00986.
3. Y. Gao, H. Li, J. Tong, and L. Wang, *Environ. Technol.*, DOI: 10.1080/09593330.2019.1701569.
4. Z. Lu, X. Lin, J. Zhang, W. Dai, B. Liu, G. Mo, J. Ye, and J. Ye, *Electrochim. Acta*, 295 (2019) 514.
5. K. Zhang, N. Zhang, H. Wang, H. Shi, Q. Liu, C. Wang, T. Geng, and G. Zhu, *Int. J. Electrochem. Sci.*,14 (2019) 10248.
6. O. J. Kingsford, D. Zhang, Y. Ma, Y. Wu, and G. Zhu, *J. Electrochem. Soc.*, 166 (2019) B1226.
7. M. H. Ghanbari, A. Khoshroo, H. Sobati, M. R. Ganjali, M. Rahimi-Nasrabadi, and F. Ahmadi, *Microchem. J.*, 147 (2019) 198.
8. B. Thirumalraj, S. Kubendhiran, S.-M. Chen, and K.-Y. Lin, *J. Colloid Interface Sci.*, 498 (2017) 144.
9. Y. Zhang, W. Lei, Y. Xu, X. Xia, and Q. Hao, *Nanomaterials*, 6 (2016) 178.
10. B. Dalkıran, P. E. Erden, C. Kaçar, and E. Kılıc¸ *Electroanalysis*, 31 (2019) 1.
11. M. Salajegheh, M. Kazemipour, M. M. Foroghi, and M. Ansari, *Electroanalysis*, 30 (2018) 1.
12. S. Kojima, F. Nagata, M. Inagaki, S. Kugimiya, and K. Kato, *RSC Adv.*, 9 (2019) 10832.
13. B. N. Chandrashekar, W. Lv, G. K. Jayaprakash, K. Harrath, L. W. Y. Liu, and B. E. K. Swamy, *Chemosensors*, 7 (2019) 24.
14. B. Zhang, J. Zhang, Y. Lin, M. Liu, G. Fang, and S. Wang, *J. Alloys Compd.*, 81 (2020) 152643.
15. Ç. C. Koçak, Ş. U. Karabiberoğlu, and Z. Dursun, *J. Electroanal. Chem.*, 853 (2019) 113552.
16. B. N. Chandrashekar, B. E. Kumara Swamy, M. Pandurangachar, T. V. Sathisha, and B. S. Sherigara, *Colloids Surf., B*, 88 (2011) 413.
17. N. Maleki, S. Kashanian, M. Nazari, and N. Shahabadi, *Biotechnol. Appl. Biochem.*, 66 (2019) 502.
18. G. B. Zhu, H. Sun, J. J. Qian, X. Y. Wu, and Y. H. Yi, *Anal. Sci.*, 33 (2017) 917.
19. A. Radi, N. Abd El-Ghany, and T. Wahdan, *Electroanalysis*, 28 (2016) 1112.
20. L. Wang, P. Huang, J. Bai, H. Wang, L. Zhang, and Y. Zhao, *Int. J. Electrochem. Sci*., 2 (2007) 123.
21. D. P. Santos, M. A. G. Trindade, R. A. G. Oliveira, M. E. Osugi, A. R. Bianchi, and M. V. B. Zanoni, *Color. Technol*., 130 (2013) 43.
22. D. P. Santos, M. F. Bergamini, V. A. F. F. M. Santos, M. Furlan, and M. V. B. Zanoni, *Anal. Lett.*, 40 (2007) 3430-3442.
23. S. Yazdanparast, A. Benvidi, M. Banaei, H. Nikukar, M. D. Tezerjani, and M. Azimzadeh, *Microchim. Acta*, (2018) 185.
24. S. Seher, A. Shah, F. J. Iftikhar, J. Nisar, M. N. Ashiq, M. A. Aljar, and M. S. Akhter, *J. Electrochem. Soc.*, 167 (2020) 027506.
25. K. V. Harisha, B. E. K. Swamy, P. S. Ganesh, and H. Jayadevappa, *J. Electroanal. Chem.*, 832 (2018) 486.
26. S. Chitravathi, B. E. K. Swamy, G. P. Mamatha, and B. N. Chandrashekar, *J. Mol. liq.*, 172 (2012) 130.
27. W. N. Hu, D. M. Sun, and W. Ma, *Electroanalysis*, 22 (2010) 584.
28. X. Wang, F. Zhang, J. Xia, Z. Wang, S. Bi, L. Xia, Y. Li, Y. Xia, and L. Xia, *J. Electroanal. Chem.*, 738 (2015) 203.
29. L. Zhang and J. Lian, *J. Solid State Electrochem.*, 12 (2008) 757.
30. J. Yang, X. Wang, and H. Shi, *Sens. Actuators, B*, 162 (2012) 178.
31. R. Sakthivel, B. Mutharani, S.-M. Chen, S. Kubendhiran, T.-W. Chen, F. M. A. Al-Hemaid, M. A. Ali, and M. S. Elshikh, *J. Electrochem. Soc*., (2018) 165, B422.
32. A. T. Ezhil Vilian, and S.-M. Chen, *RSC Adv*., 4 (2014) 55867.
33. M. F. Bergamini, D. P. Santos, and M. V. B. Zanoni, *Bioelectrochemistry*, 77 (2010) 133.
34. M. F. Bergamini, D. P. Santos, and M. V. B. Zanoni, *J. Braz. Chem. Soc*., 20 (2009) 100.
35. S.-Y. Yi, J.-H. Lee, and H.-G. Hong, *J. Appl. Electrochem.*, 44 (2014) 589.
36. F. Zhang, Z. Wang, Y. Zhang, Z. Zheng, C. Wang, Y. Du, and W. Ye, *Talanta*, 93 (2012) 320.

37. W. Qiao, L. Wang, B. Ye, G. Li, and J. Li, *Analyst*, 140 (2015) 7974.
38. X. Ma, M. Chen, H. Lv, Z. Deng, M. Yin, and X. Wang, *Int. J. Electrochem. Sci.*, 13 (2018) 6286.
39. H. Gao, Q. Q. Hu, W. Ma, Y. M. Wang, W. T. Chen, and D. M. Sun, *Rev. Roum. Chim.*, 64 (2019) 809.
40. Z. Chen, Z. Zhang, C. Qu, D. Pan, and L. Chen, *Analyst*, 137 (2012) 5197.
41. P. Jakszyn and C. A. Gonzalez, *World J. Gastroenterol.*, 12 (2006) 4296.
42. V. Y. Titov and Y. M. Petrenko, *Biochemistry*, 70 (2005) 473.
43. A. Aschengrau, S. Zierler, and A. A. Cohen, *Arch. Environ. Health*, 44 (1989) 283.
44. C. W. Kung, T. H. Chang, L. Y. Chou, J. T. Hupp, O. K. Farha, and K. C. Ho, *Electrochem. Commun.*, 58 (2015) 51.
45. Q. H. Wang, L. J. Yu, Y. Liu, L. Lin, R. G. Lu, J. P. Zhu, L. He, and Z. L. Lu, *Talanta*, 165 (2017) 709.
46. Z. Xia, Y. Zhang, Q. Li, H. Du, G. Gui, and G. Zhao, *Int. J. Electrochem. Sci*., 15 (2020) 559.
47. Z. Xia, Y. Zhang, D. Gao, H. Xiong, Y. Gao, S. Li, X. Li, Z. Yang, M. Liu, J. Dai, and D. Zhang, *Int. J. Electrochem. Sci*., 14 (2019) 506.
48. S. Li, J. Qu, Y. Wang, J. Qu, and H. Wang, *Anal. Methods*, 8 (2016) 4204.
49. B. Ding, H. Wang, S. Tao, Y. Wang, and J. Qiu, *RSC Adv.*, 6 (2016) 7302.
50. M. Shivakumar, K. L. Nagashree, S. Manjappa, and M. S. Dharmaprakash, *Electroanalysis*, 29 (2017) 1434.
51. Y. Ma, X. Song, X. Ge, H. Zhang, G. Wang, Y. Zhang, and H. Zhao, *J. Mater. Chem. A*, 5 (2017) 4726.
52. W. Q. Wu, Y. B. Li, J. Y. Jin, H. M. Wu, S. F. Wang, Y. Ding, and J. F. Ou, *Microchim. Acta*, 183 (2016) 3159.
53. Y. Haldorai, S. K. Hwang, A. I. Gopalan, Y. S. Huh, Y. K. Han, W. Voit, G. Sai-Anand, and K. P. Lee, *Biosens. Bioelectron.*, 79 (2016) 543.
54. C. W. Kung, Y. S. Li, M. H. Lee, S. Y. Wang, W. H. Chiang, and K. C. Ho, *J. Mater. Chem. A*, 4 (2016) 10673.
55. L. H. Chen, X. Liu, C. G. Wang, S. L. Lv, and C. F. Chen, *Microchim. Acta*, 184 (2017) 2073.
56. Z. Li, Z. An, Y. Guo, K. Zhang, X. Chen, D. Zhang, Z. Xue, X. Zhou, and X. Lu, *Talanta*, 161 (2016) 713.
57. D. Chen, J. J. Jiang, and X. Z. Du, *Talanta*, 155 (2016) 329.
58. D. M. Stankovic, E. Mehmeti, J. Zava-nik, and and K. Kalcher, *Sens. Actuators, B*, 236 (2016) 311.
59. S. F. Jiao, J. Jin, and L. Wang, *Sens. Actuators, B*, 208 (2015) 36.
60. H. Liu, K. Guo, J. Lv, Y. Gao, C. Y. Duan, L. Deng, and Z. F. Zhu, *Sens. Actuators, B*, 238 (2017) 249.
61. G. Wang, H. Huang, G. Zhang, X. Zhang, B. Fang, and L. Wang, *Anal. Methods*, 2 (2010) 1692.
62. R. K. Shervedani and S. A. Mozaffari, *Anal. Chem.*, 78 (2006) 4957.
63. J. Li, H. Feng, Y. Feng, J. Liu, Y. Liu, J. Jiang, and D. Qian, *Microchim. Acta*, 181 (2014) 1369.
64. J. Wu, L. Wang, Q. Wang, L. Zou, and B. Ye, *Talanta*, 150 (2016) 61.
65. G. A. DiLabio, and E. R. Johnson, *J. Am. Chem. Soc.*, 129 (2007) 6199.
66. A. Takai, C. P. Gros, J.-M. Barbe, R. Guilard, and S. Fukuzumi, *Chem. - Eur. J.*, 15 (2009) 3110.
67. E. Laviron, *J. Electroanal. Chem*., 52 (1974) 355.
68. P. K. Sonkar and V. G*anesan, J. Solid State Electrochem.*, 19 (2015) 2107.
69. X. Y. Liu, Y. H. Li, X. S. Liu, X. D. Zeng, B. Kong, S. L. Luo, and W. Z. Wei, *J. Solid State Electrochem.*, 16 (2012) 883.